Optical Engineering

SPIEDigitalLibrary.org/oe

Miniaturized suspension structure for precise flying height positioning measurement using a swing arm actuator with a holographic optical element module sensor

Po-Chien Chou
Yu-Cheng Lin
Stone Cheng

Miniaturized suspension structure for precise flying height positioning measurement using a swing arm actuator with a holographic optical element module sensor

Po-Chien Chou
Yu-Cheng Lin
Stone Cheng
National Chiao Tung University
Department of Mechanical Engineering
1001 University Road
Hsinchu, 300 Taiwan
E-mail: stonecheng@mail.nctu.edu.tw

Abstract. This work presents a means of active actuation of the suspension structure with a holographic optical element (HOE) for the small-form-factor optical-disk drives. The proposed HOE module sensor is mounted on a swing arm swivel-drive mechanism with unique features, including a rotary actuator for tracking and a swing arm nutates along a pivot for focusing. The fabrication methodology for a cantilever-beam-like structure with HOE module sensor is investigated. Furthermore, the performances of optical module with swing arm-swivel actuation are experimentally evaluated to demonstrate the effectiveness of precise flying height positioning measurement method. [DOI: 10.1117/1.3549259]

Subject terms: swing arm actuator; HOE module sensor; small-form-factor; focus error signal.

Paper 100764RR received Oct. 15, 2010; revised manuscript received Dec. 23, 2010; accepted for publication Jan. 10, 2011; published online Mar. 1, 2011.

1 Introduction

Current small form factor technologies offer potential solutions for obtaining high data capacity. A proposed implementation combines short wavelength laser diodes and high numerical aperture lens integrated in a micro-optical pickup and actuated by a biaxial swing arm type actuator.

Literature reviews of works in generating miniaturized optical storage devices indicate that most works focus on optical architecture design and analysis to meet optical requirements,[1–3] but few studies have considered actuator performance simultaneously. The important drive specifications of the mechanical system, which consists of the spindle, swing arm, and the voice coil motor, have not been discussed. New technologies have minimized the number of optical components needed and have simplified the light path to enhance optical efficiency. This study proposes a holographic optical element (HOE) module sensor design combined with a swing arm mechanism to make an accurate measurement of disk information, which is developed to meet typical optical specifications. However, aligning and centering optics employed in an optical system poses different challenges depending on the required precision. A technique for accurately aligning optical systems is described to establish a standardized process for assembling an integrated pickup unit,[4] which employs high precision packaging without affecting the components performance. Another issue of the integrated unit assembly is the focus error signal (FES) generated by a biaxial actuator.[5] This special requirement of the flying head employs very small, lightweight components to obtain a compact mechanical system.[6–8] However, when the disk surface oscillates during rotation, the laser beam is reflected along a different path. The disk surface vibration leads the position of the beam spot to produce disturbances on the photodetector. This study fabricated a swing arm mechanism with a focusing mechanism to perform the stable sensing operation. The swing arm actuator was designed on the basis of electromagnetic (EM) and finite element (FE) structural analyses for both focus/tracking actuations.[9–13] To maximize the swing arm actuator driving force, a magnetic circuit with a fan-shaped-type magnet for the tracking motion was suggested.[14–16] Based on the HOE module sensor for focusing motion and a swing arm swivel actuator that performs precise positioning, the proposed measurement method for stable flying height is feasible.

2 Overview of Micro-Optical Pickup Head Assembly

This work describes a small-form-factor (SFF) optical configuration design using an HOE based on the optical specifications in Table 1. The fabrication processes of this HOE module sensor are illustrated in Fig. 1. The proposed devices are fabricated and tested to demonstrate the unique performances and advantages.[17,18] Nonetheless, the thermal dissipation of the blue violet laser diode prevents the acquisition of good current-voltage characteristics by controlling the optical power density distribution in the optical region. Therefore, 635-nm laser assembly technologies are expected to play an important role in stabilizing new holographic pickup structures. The proposed optical unit consists of a 635-nm edge-emitting laser diode chip, a submount, a 45 deg turning mirror, two microprisms, a HOE, a quadrant photodetector (PD), and a objective lens module (objective lens and lens holder). The optical layout of a laser module with the HOE is using the astigmatic focus detection method. Figure 2 and Table 2 show that the HOE acts as both a beam splitter and a cylindrical lens for generating the diffraction beam and astigmatic focus error signal.

0091-3286/2011/$25.00 © 2011 SPIE

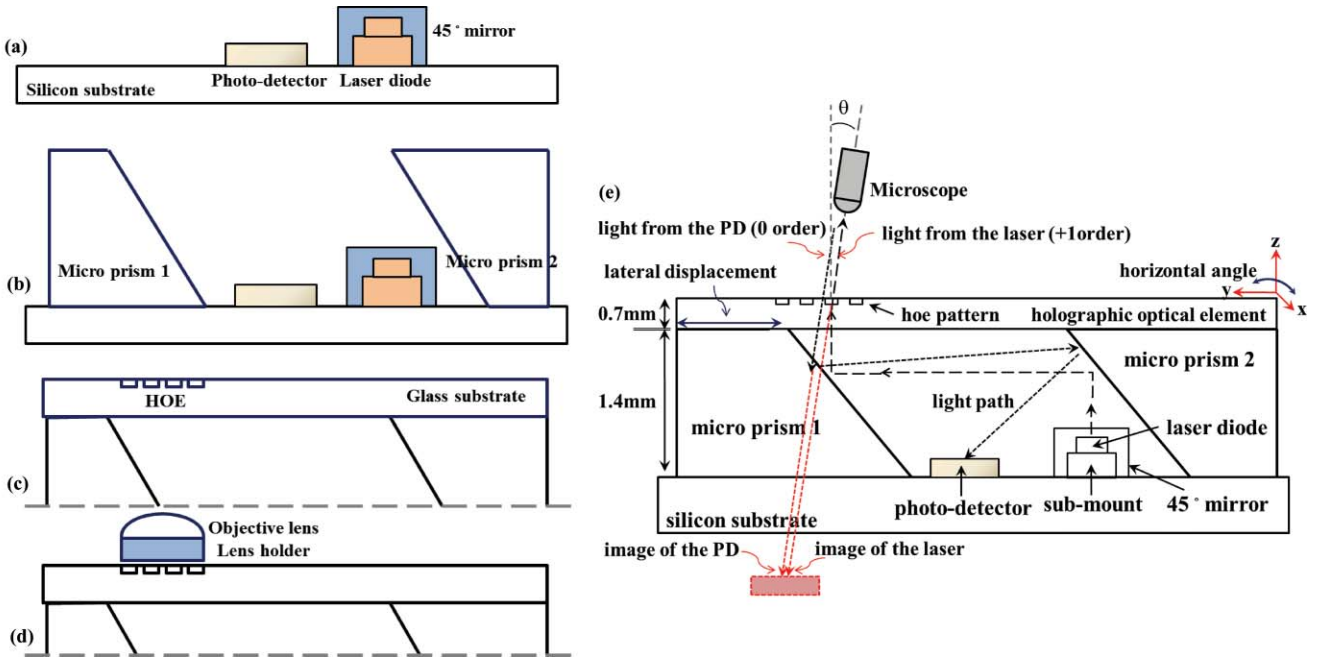

Fig. 1 Fabrication processes of the HOE module sensor. (a) Laser diode, photodiode, and turning mirror; (b) microprisms; (c) HOE glass substrate; (d) objective lens modulus; and (e) virtual image method of HOE alignment.

Table 1 Optical specifications of HOE module sensor.

Item	Correspondence
Image object relation	Finite-conjugate system
Laser wavelength	635 nm
Object NA (laser side)	0.1
Image NA (disk side)	0.65
Focal length	0.525 mm
Clear aperture diameter	1.0 mm
Dimensions	3.1 mm (H) × 3 mm (W) × 5 mm (L)
Tracking error signal detection	Push–pull method
Focusing error signal detection	Astigmatic method

Table 2 Summary of diffraction angle and efficiency of diffractive spots.

	Diffraction angles		Diffraction efficiency	
	Calculated	Measured	Calculated	Measured
Zero order	0°	0°	40%	38%
First order	7.34°	7.5°	20%	18%

The following descriptions are the optical layout of the HOE module sensor. After the 45 deg turning mirror reflects the horizontal laser beam upward, microprisms 2 and 1 redirect the beam upward to the HOE. After the reflected beam enters the HOE perpendicularly, the zero-order laser beam passes through the objective lens and focuses on the disk. The HOE was proposed as a beam-splitting element to simplify optical path and the optical components. On the optical return path, the returning beam is diffracted by the HOE patterns and reflected by microprism 1 to microprism 2. The microprisms provide support substrates as well as calibration reference planes based on the virtual image method. Finally, the returning beam projected on the quadrant PD generates the FES, tracking error signal, and radio frequency signal from the HOE diffraction.

The assembly process for an HOE module sensor requires precise alignment to meet position tolerances. Because optical components are intended to manipulate light to the desired

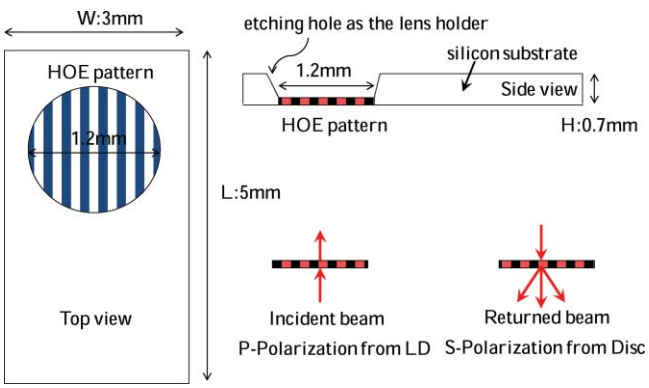

Fig. 2 HOE dimensions and specifications.

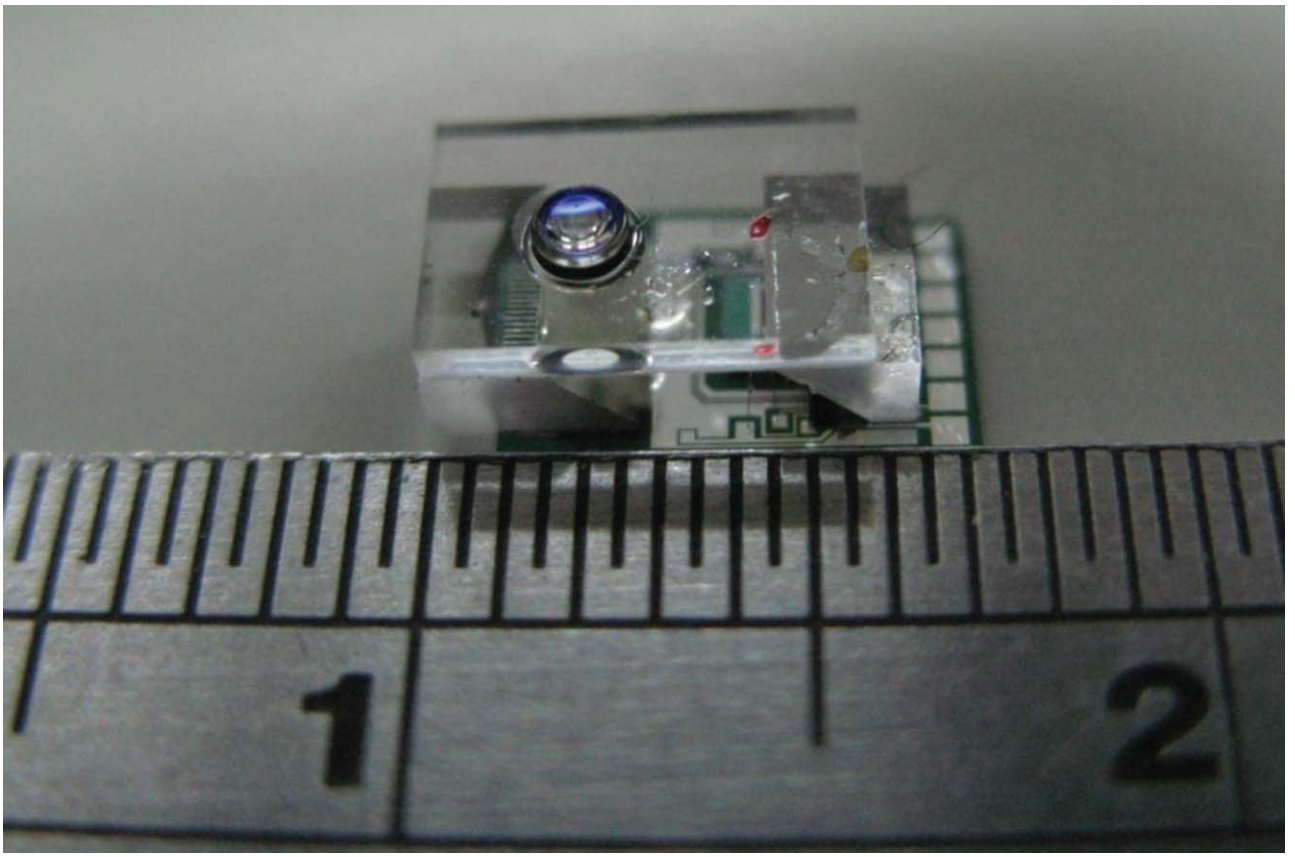

Fig. 3 Integrated optical module for SFF pickup unit.

location, the most important operational process during SFF pickup assembly is the precise attachment of a temperature-sensitive laser diode. Threshold current and operating temperature characteristics are crucial factors in laser diode (LD) lifetime as increasing operating temperature also increases threshold current. Because SFF size constraints limit heat convection, heat transfer phenomena and other thermal considerations should be considered in system design. Therefore, edge-emitting LD operating at a high current requires a heat sink between the device active region and the silicon substrate. The high thermal conductivity of thin film metal-dielectric enables use in diode submount applications.

The distance from the edge of the submount to the LD emitting facet is a key factor in the bonding of diodes mounted with their P-sides face down.[19] In the high precision eutectic process, the LD emitting edge must be placed within a few micrometers from the edge of the submount. A diode bonded to the inner side of the submount partially blocks the emitting beam and reduces brightness. Conversely, if a diode is bonded too far away from the edge of the submount, the generated heat may reduce optical performance and shut down the diode. To maximize the lifetime of the laser diode, the laser emitting facet must be properly aligned with the edge of the submount. The laser subassembly must be precisely positioned with respect to other components along the optical axis. When the LD is mounted, the laser establishes a reference for the optical axis, and the turning mirror and two microprisms must accordingly be positioned in Fig. 3.

The virtual image method was used to obtain a reliable system alignment. The schematic diagram in Fig. 4 shows that a passive alignment procedure can be used to adjust the corresponding distance between the photodetector and HOE. The virtual image used as a calibration point was obtained by extending the first order diffracted beam backward to the virtual focal point. This point must coincide with the locations of the photodetector image and the laser spot virtual image observed by the microscope. Because the HOE and other integrated units were aligned in the established light path, optical alignment was performed by adjusting the lateral displacement of microprism 1 and rotating the horizontal angle of the HOE glass in a specific clamping apparatus with a tilted microscope; that is, the alignment tolerances among the LD, turning mirror, and microprism assembly be removed.

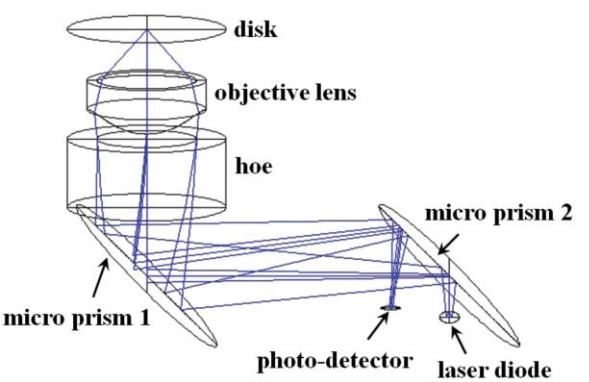

Fig. 4 Layout of the optical path in HOE module.

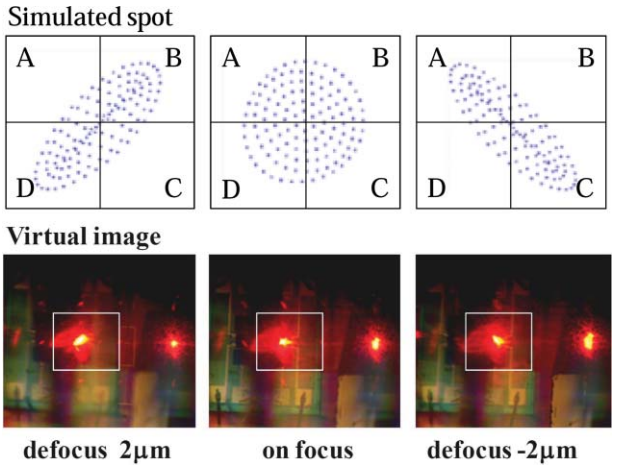

Fig. 5 Simulation and experimental images of astigmatic returning spot on the quadrant detector.

Figure 5 shows the observed virtual image adjustment consisting of the spot center on the quadrant detector and the shape of the astigmatic returning spots. Simulated spots are also shown for comparison.

After attaching the microprisms and the HOE to the optical module, the objective lens unit was assembled. The interferometer and mechanical gripping stage were used to assemble the objective lens unit on the optical module. The assembly was performed using a precision modular platform with a 2-axis rotational degrees of freedom and 3-axis translation to minimize aberrations such as coma, astigmatism, and spherical aberration. Finally, an ultraviolet curable epoxy was used to attach the integrated subassembly to the objective lens module.

3 Swing Arm Swivel Actuator Design

Large optical heads hampered the use of swing arm actuators in optical recording. Using a miniature integrated HOE module on the actuator, therefore, can overcome this limitation. The DataPlay actuator with tilt and rotary actuation consisted of a swing arm, pickup head, suspension, hinge spring, and voice coil motor (VCM).[20] The swing arm with carbon fiber was pinned with a bearing and mounted with a VCM to provide tracking motion.[21] The arm was also connected to the suspension by a hinge spring. A VCM was mounted at the center of the front suspension. The optical pickup unit (OPU) at the tip of the suspension can be controlled to provide the focusing motion. Many proposed approaches use the swing arm type to realize the microstorage system.[22] To improve the structural properties of the swing arm, one solution was using a three-layer structure of steel-aluminum-steel.[23] Although this structure provided the swing arm with high heat thermal conductivity, the module required additional working hours to manufacture, which increased product cost. The added stress between the suspension and swing arm also reduced mechanical durability. Under normal operating conditions, the hinge springs were susceptible to permanent fracture.

Accordingly, the actuator suspension was improved in two ways. One was increasing the second torsion mode to limit the servo bandwidth of the actuating range. The other was decreasing hinge spring stress concentration and thermal conductivity. Common methods of increasing the above swing arm actuator parameters include using materials with high Young's modulus and low density, such as alumni alloy, and by strengthening the stiffness of load suspension with embossments to optimize suspension shape.[24] Durability was improved by designing a swing-type rotary VCM actuator without a hinge spring to provide the miniaturization and smooth focusing motion. The conventional hinge required sufficient robustness to support the weight of pickup head and suspension. However, the single-arm swing arm mechanism also increased strength and torque.

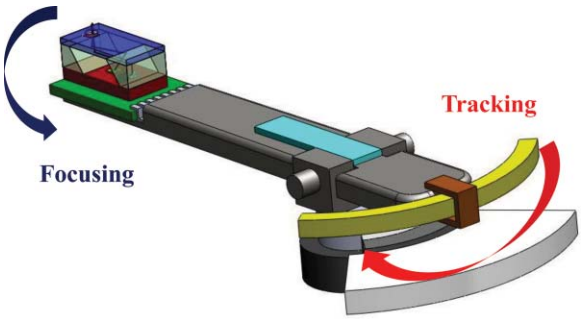

Fig. 6 Overall structure and motion of swing-type rotary VCM actuator with HOE module sensor.

Figure 6 shows the overall structure of the swing arm actuator. The aluminum alloy swing arm was connected to two steel balls by the fixed cylinder pins. The cylinder pin restricted the ball, which contacted the side of the arm and provided one degree of freedom in vertical axis (with the direction of the pin clamped). The sleeve in the middle of the swing arm also held the frame and rotated to provide horizontal movement. Moreover, the VCMs were glued at the bottom and on the back side of the arm. Current flowing to both coils produced the moment around the axial base. Hence, the swing arm for the optical module had a tilting motion in the focusing direction and a rotating motion in the tracking direction. A spring damper clamped in the gap of the frame provided a horizontal balance. The advantages of this design were as follows. First, the total weight of the moving parts was lighter than that of any other parts of an actuator with a hinge spring. The leverage magnified the VCM driving force to achieve a high focusing effect. Second, reinforcing the actuator with aluminum alloy instead of triple layers increases the lateral stiffness. Finally, the total mass of moving parts was counterbalanced in the fulcrum of the arm, and the stress energy distribution was reduced to maximize system sensitivity. Notably, a ring yoke through the tracking coils not only provided uniform magnetic flex, but also restricted the rotator angle of the arm. The focus working distance was limited to ± 0.2 mm, which was shorter than the 0.525 mm (effective focal length) needed to avoid abrupt impacts on the head that might damage the disk.

4 Swing Actuator Simulations and Experiments

The design process of a swing arm is optimized for the swing-type actuator in order to guarantee the tracking and focusing stability. Hence, FE simulation was performed using ANSYS 10.0. Figure 7 shows the FE model and mode shapes of the swing-arm, and Table 3 shows the frequency results. A frequency range of 0 to 10 kHz was measured because it is the common nature frequency span of mechanism structure, and the objectives were five different resonance modes I to V. The cantilever mode (mode I) obtained a frequency of 1285.6 Hz, which was a substantial improvement.

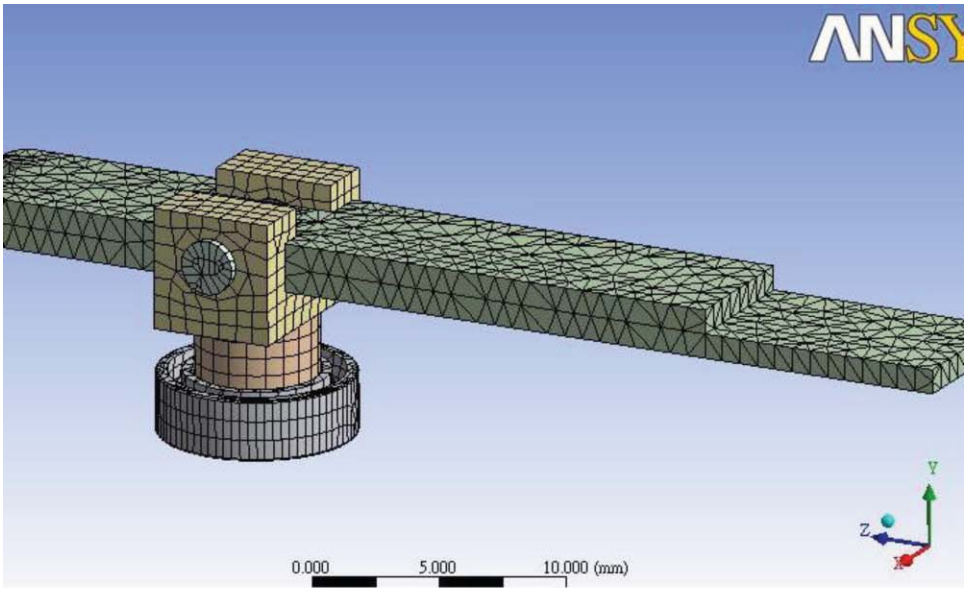

(a)

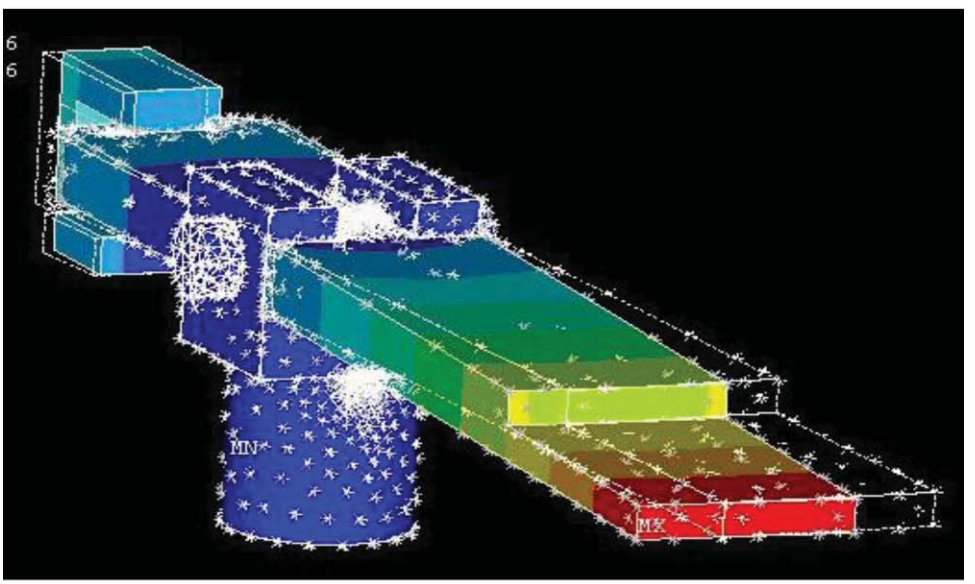

(b)

Fig. 7 FE model (a) and vibrational mode I shape (b) of swing-type rotary VCM actuator.

Table 3 Resonance frequency modes characteristics.

Mode	Resonance frequency	Response
I	38 Hz	cantilever
II	1285.6 Hz	1st bending
III	2531 Hz	2nd bending
IV	5174 Hz	1st torsion
V	7648 Hz	2nd torsion

Figure 8 shows the proposed fabricated swing-shaped rotary VCM actuator with HOE module sensor. The swing arm, frame, and sleeve were constructed of aluminum alloy to reduce magnetic influence between EM circuits, the yokes were made from low carbon steel, and the magnet arrays were made from NdFeB.

Figure 8 also shows the experimental apparatus of the Dynamic measurement. The relative displacement of the fabricated actuator was measured by a laser doppler vibrometer. A dynamic signal analyzer (DSA) transformed input and output time-domain signals to frequency response. The performance of the fabricated actuator was assessed by tests of dynamic tracking and focusing motion. Figure 9 shows the frequency response of the swing actuator. The dc sensitivity in focusing direction is 0.194 mm/V. The mode I and

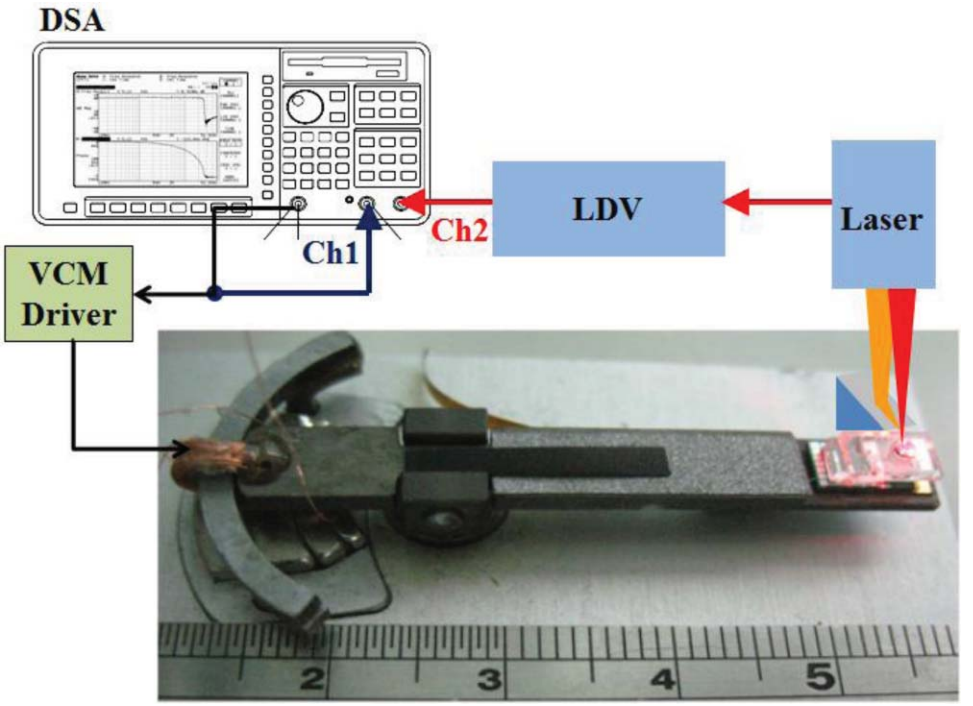

Fig. 8 Experimental apparatus and fabricated swing-arm actuator equipped with HOE module sensor. The dynamic response of focusing and tracking motions are measured by DSA(Ch2/Ch1).

cantilever mode frequencies were about 30 Hz. The cantilever mode shown in the Bode plot [Fig. 9(a)] was consistent with the computer simulation and had a small resonance peak. The actuator had a first bending mode of 3.85 kHz in focusing direction and was not apparent in the Bode plot. In the simulation, however, it had a second resonance frequency of 4 kHz. This frequency was obtained by the manufacturing process using meshing tools and assembled techniques. In an actuator fabricated using a technical method, the frequency of first bending mode may resemble that in the simulation. Hence, the swivel actuator is promising for the measurement of tiny displacements.

5 Optical Pickup Head Experiments

Figure 10 shows the measurement of focusing spot size with radial and tangential spot distributions with the objective lens attached. Although the full-width at half-maximum (FWHM) spot size in the disk radial direction exceeded that in the tangential direction, the spot intensity was normally distributed and aberrations were within the acceptable range. The difference in FWHM between the tangential and radial dimensions was about 2%.

The experimental setup for analyzing the performance of the integrated SFF optical device included an integrated SFF pickup unit, a swing-type actuator, an optical signal conversion amplifier, and a mini disk media. The quadrant detector employed an astigmatic method for focusing detection and a push–pull method for tracking detection. Table 4 shows the PD layout and specifications. Figure 11 also shows four segmented cells for extracting the FES and RF (A, B, C, and D). The FES and RF were calculated using the following formulas:

$$\text{Focus Error Signal} = (\text{A} + \text{C}) - (\text{B} + \text{D}),$$

$$\text{RF Signal} = \text{A} + \text{B} + \text{C} + \text{D}.$$

Figure 12 shows the measurement and simulation results of the nearly symmetrical S-curve obtained by the astigmatic focusing method, where the horizontal axis represents the actuation displacements applied to the swing swivel actuator and the vertical axes are the output voltages of the op-amp circuit. The linear range in the focusing direction is about 4 μm. The tolerable balance of the measured S-curve was obtained using the following formula:

$$\text{Balance of S-curve} = \left| \frac{\text{V}_{\text{peak}} - \text{V}_{\text{bottom}}}{2(\text{V}_{\text{peak}} + \text{V}_{\text{bottom}})} \right| \times 100\% < 10\%.$$

The S-curve balance was 9.5%, which did not exceed the maximum tolerance of 10%. Also, to verify the focusing performance of this HOE module sensor, the focusing actuator was driven by a 20–Hz triangular signal with a magnitude of ± 140 mV to bring the optical module passes to its focus point to the disk. Figure 13 shows the S-curve of the focusing error signal which indicated that the measured results are satisfactory and demonstrated the feasibility of the HOE module sensor.

6 Conclusions

This study proposed a miniaturized suspension structure for precise flying height positioning measurement using a swivel actuator with HOE module sensor in small form factor applications. To ensure proper operation of the HOE module sensor, attaching the temperature-sensitive laser diode required precision assembly processes to align the laser emitting facet accurately. After establishing the reference optical path, the

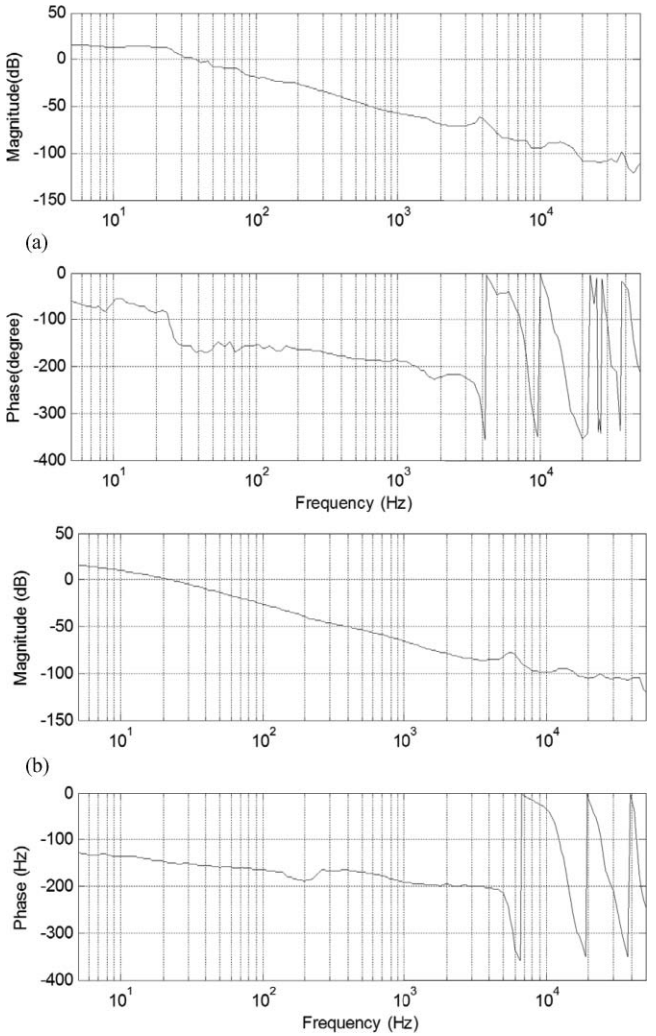

Fig. 9 Frequency responses of fabricated swing actuator. (a) Focusing direction and (b) tracking direction.

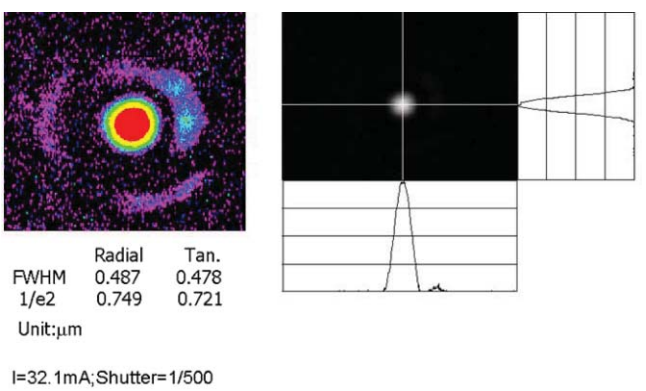

Fig. 10 Measurement of the focused spot size.

virtual image method with HOE pattern alignment was performed to achieve a stabilized focus of the servo function. A swing arm actuator was also developed to drive the HOE module sensor; this accurate lever mechanism magnified the focusing force and strengthened the stiffness of load suspension. The effect of the driving force on this actuator was studied to clarify the biaxial performance. A seesaw swivel

Table 4 Specifications of split PD.

Specification
Breakdown voltage $>$ 10V
Sensitivity $>$ 0.4 A/W (635 nm)
Dark current 2 nA
Crosstalk $<$ 15% (gap 5 μm)
Rise time & fall time $<$ 5 ns for center detecting elements

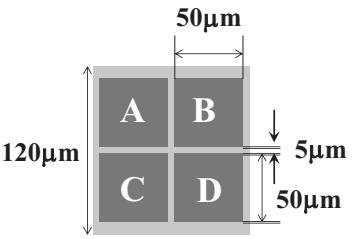

Fig. 11 The size of the PD pattern.

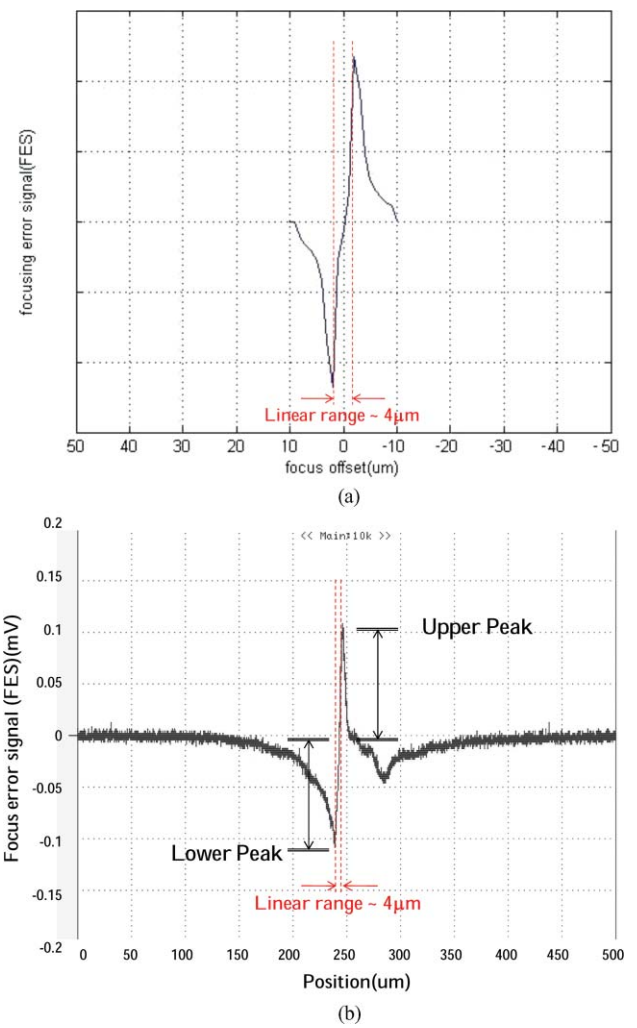

Fig. 12 Focusing error signal (S-curve). (a) Simulation and (b) measurement.

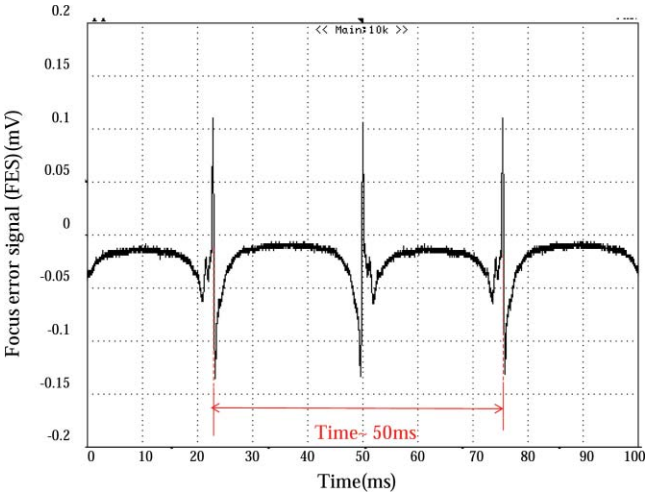

Fig. 13 Measured focus error signal during actuator focusing motion (at 20 Hz).

actuator is well suited for a miniature optical module to have the nutating actuation to maintain the predetermined flying height and to permit rapid disk rotation, which can be applicable to SFF CD/DVD/BD drives. Finally, the fabricated apparatus for measurement was evaluated by dynamic experiments in the tracking and focusing direction. The actuation performance, the radial and tangential spot distributions, and the focus performance of tolerable S-curve balance (9.5%) for precise flying height positioning measurement were verified.

Acknowledgments

The authors would like to thank the Ministry of Economic Affairs of the Republic of China, Taiwan, under the TDPA project (Contract No. MOEA98-EC-17-A-07-S1–011) and the National Science Council of the Republic of China, Taiwan (Contract No. NSC 96–2221-E-009–149) for financially supporting this research.

References

1. D. L. Blankenbeckler, B. W. Bell, K. Ramadurai Jr., and R. L. Mahajani, "DataPlay's small form-factor optical disc and drive," *Jpn. J. Appl. Phys.* **45**, 1181–1186 (2006).
2. S. Kim, J. M. Park, H. Jeong, G. Park, J. Y. Kim, J. Choi, and Y. Yee "Design and fabrication technology of optical flying head for first surface magneto-optical recording," *Jpn. J. Appl. Phys.* **42**, 1018–1021 (2003).
3. M. Song, J. H. Woo, N. C. Park, J. Yoo, Y. P. Park, and K. S. Park, "Design of the rotary VCM actuator for small form factor optical disk drive," *Microsyst. Technol.* **16**, 205–212 (2009).
4. H. F. Shih, "Integrated optical unit design for the collinear holographic storage System," *IEEE Trans. Mag.* **43**, 948–950 (2007).
5. C. C. Hsiao, C. Y. Peng and T. S Liu, "An optical lever approach to photodetector measurements of the pickup-head flying height in an optical disk drive," *Meas. Sci. Technol.* **17**, 2335–2342 (2006).
6. C. S. Chang, T. S. Liu, and Y. C. Tang,"A tracking motion approach for a piezotube actuator in a disk drive subject to disk deformation and disturbance," *Smart Mater. Struct.* **16**, 1542–1548 (2007).
7. S. J. Yoon, J. Lee, Y. P. Park, and D. H. Choi, "Design of optical flying head for magnetooptical recording," *IEEE Trans. Mag.* **41**, 2851–2853 (2005).
8. S. Kim, S. J. Yoon, D. H. Choi, and S. Y. Lee, "A study on the flying stability of optical flying head on the plastic disks," *IEEE Trans. Mag.* **41**, 986–988 (2005).
9. P.-C. Chou, Y.-C. Lin, and S. Cheng, "Optimization of seesaw swing arm actuator design for small form factor optical disk drive," *Jpn. J. Appl. Phys.* **49**, 052502 (2010).
10. P.-C. Chou, Y.-C. Lin, and S. Cheng, "A novel seesaw swivel actuator design and fabrication," *IEEE Trans. on Mag.* **46**, 2603–2610 (2010).
11. Y. Tang, S. X. Chen, and L. S. Low, "Micro electrostatic actuators in dual-stage disk drives with high track density," *IEEE Trans. Mag.* **32**, 3851–2853 (1996).
12. J. R. Edwards, "Finite element analysis of the shock response and head slap behavior of a hard disk drive," *IEEE Trans. Mag.* **35**, 863–867 (1999).
13. D. J. Lee, G. W. Jung, N. C. Park, H. S. Yang, Y. P. Park, B. Y. Song, W. I. Cho, P. Y. Seong, and K. H. Lee, "Coupled-field-analysis and dynamic improvement of ultraslim optical pickup actuator," *Jpn. J. Appl. Phys.* **44**, 3373–3378 (2005).
14. J. Jeong and D.-G. Gweon, "Optimal design of rotary-type voice coil motor using multisegmented magnet arrayfor small form factor optical disk drive," *Jpn. J. Appl. Phys.* **46**, 2912–2914 (2007).
15. J. Jeong, M. G. Lee, J. H. Lee, H. K. Yoon, and D. G. Gweon, "Multisegmented magnet array on voice coil motor in rotating data storage devices," *Jpn. J. Appl. Phys.* **43**, 1398–1402 (2004).
16. M. G. Lee, J. Jeomg, and D. G. Gweon, "A comparative analysis of voice cmotors with multisegmented and conventional magnet arrays for rotating data storage devices," *Jpn. J. Appl. Phys.* **42**, 3394–3395 (2003).
17. Y. Chiu, H. F. Shih, J. C. Chiou, S. T. Cheng, K. Y. Hung, F. G. Tseng, and W. Fang, "Design and fabrication of a small-form-factor optical pickup head," *IEEE Trans. Mag.* **45**, 2194–2197 (2009).
18. S. Kim, J. Park, G. Park, J. Lee, J. Lee, H. Jung, J. Y. Kim, S. H. Kim, Y. Yee, J. H. Kim, J. H. Kim, and J. Bu, "An optical flying head assembly for a small-form-factor plastic disk in PCMCIA-like drive," *Jpn. J. Appl. Phys.* **43**, 4752–4758 (2004).
19. H. F. Shih, T. P. Yang, M. O. Freeman, J. K. Wang, H. F. Yau, and D. R. Huang, "Holographic laser module with wavelwngth for digital versatile disc optical Heads," *Jpn. J. Appl. Phys.* **38**, 1750–1754 (1999).
20. D. L. Blankenbeckler, B. W. Bell, Jr., D. H. Davies, and L. W. Lee, "Performance characteristics of a 32mm small form-factor optical disc and drive," *Jpn. J. Appl. Phys.* **43**, 4896–4899 (2004).
21. K. Suzuki, S. Tsuda, T. Deguchi, and T. Shimizu, "VCM design with round coil and axe-shaped magnet for hard disk drive actuator," *Microsyst. Technol.* **13** 1093–1101 (2007).
22. D. J. Lee, S. J. Park, J. Oh, N. C. Park, Y. P. Park, and H. S. Jung, "Development of rotary-type voice coil motor actuator for small-form-factor optical disk drive," *Jpn. J. Appl. Phys.* **45**, 1124–1128 (2006).
23. D. J. Lee, J. H. Woo, S. U. Kim, J. S. Oh, J. H. Yoo, N. C. Park, Y. P. Park, T. Shimano, and S. Nakamura, "Development of "L-shaped" rotary voice coil motor actuator for ultra slim optical disk drive using integrated design method based on coupled-field analysis," *Jpn. J. Appl. Phys.* **46**, 3715–3723 (2007).
24. K. Ishioka, N. Kojima, K. Takahashi, and K. Watanabe, "Novel suspension structure for near-field optical recording system," *IEE Proc.-Sci. Meas. Technol.* **150**, 198–201 (2003).

Biographies and photographs of the authors not available.